18 D

PNL-2456

UC-66d

Corrosion of Iron-Base Alloys Versus Alternate Materials in Geothermal Brines

Interim Report-
Period Ending October 1977

by
Donald W. Shannon

November 1977

Prepared for the
U.S. Department of Energy
under Contract EY-76-C-06-1830

Battelle
Pacific Northwest Laboratories

PNL-2456

NOTICE

PACIFIC NORTHWEST LABORATORY
operated by
BATTELLE
for the
UNITED STATES DEPARTMENT OF ENERGY
Under Contract EY-76-C-06-1830

Printed in the United States of America
Available from
National Technical Information Service
United States Department of Commerce
5285 Port Royal Road
Springfield, Virginia 22151

Price: Printed Copy $____*; Microfiche $3.00

*Pages	NTIS Selling Price
001-025	$4.50
026-050	$5.00
051-075	$5.50
076-100	$6.00
101-125	$6.50
126-150	$7.00
151-175	$7.75
176-200	$8.50
201-225	$8.75
226-250	$9.00
251-275	$10.00
276-300	$10.25

PNL-2456
UC-66d

CORROSION OF IRON-BASE ALLOYS VERSUS ALTERNATE MATERIALS IN GEOTHERMAL BRINES
(Interim Report - Period Ending October 1977)

by
Donald W. Shannon

November 1977

BATTELLE
Pacific Northwest Laboratories
Richland, Washington 99352

CONTENTS

FIGURES

TABLES

INTRODUCTION

This geothermal corrosion program is to determine why geothermal brines are so corrosive to economical iron-base alloys. Geothermal resources that can be developed with iron-base alloys will have a significant economic advantage over geothermal sites that would require extensive use of expensive alloys. Data developed in this program will be used to guide selection and design of near-term plants.

The program objectives are:

- To clarify corrosion factors important to materials selection for geothermal power plants.
- To establish a set of brine composition and temperature limits for carbon steels in geothermal brines and report final results by the end of FY 1978.

The program involves tests of many materials in high pressure equipment where a wide variety of brine chemistries can be studied. The validity of these lab tests is checked by field tests in actual geothermal brine.

SUMMARY AND CONCLUSIONS

A series of 30 refreshed autoclave tests and one field test have been completed to define how various chemical components in geothermal brines affect uniform corrosion of 35 materials.

The data indicate uniform corrosion rates of carbon steels will be satisfactory for most major components of a geothermal power plant for low salinity, neutral to alkaline pH reservoirs, when 20 mpy (mils per year) corrosion allowances are permitted. Corrosion rates of carbon steels probably will be excessive under the following conditions:

- Carbon dioxide saturated, low pH (<pH 6) brines at ambient to 100°C temperature, and CO_2 saturated steam condensate system.
- Applications near 250°C and above in salinities above 5 to 10%.

- Thin sections such as heat exchanger tubes (may fail by pitting).
- Applications where any oxygen may be present, such as steam condenser and waste injection systems.

While some minor alloy effects were observed among the 10 carbon steels tested, the alloy composition of the carbon steel was a second order effect compared with important brine chemistry variables such as pH, salinity, and temperature. Acidification of East Mesa geothermal brine to pH 4.8 increased carbon steel corrosion 3 to 4 times in agreement with lab tests.

The corrosion rates of carbon steels were found to be largely controlled by the composition and structure of the corrosion product film that formed on the metal. These films followed thermodynamic predictions. This also means mineral scale deposits could significantly affect corrosion rates and must be investigated further.

A number of alloys were found in the screening tests that showed negligible corrosion under all conditions tested up to 250°C and 22% salinities. Alternate materials to carbon steels include: high chromium alloys above 23% Cr including E-Brite 26-1, 446, 29 Cr-4 Mo, 29 Cr-4 Mo-2 Ni, 26 Cr-1 Mo-1 Ti, Al 6X; nickel alloys Hastelloy C276, Inconel 625, Incoloy 825; four titanium alloys; and zirconium.

The tests to date only cover uniform corrosion resistance. Although no significant pitting was observed in these tests, further work needs to be done on nonuniform corrosion (pitting and crevice corrosion). All of the experimental test environments were very low in oxygen (<0.01 ppm) and contained no other ions to raise the redox potential. Slight increases in oxygen or sulfate ion could affect pitting or crevice corrosion and must be investigated further.

The tests to date have only lasted two weeks' duration. The field test lasted six weeks and will be reported in the next report. It is clear longer time testing is needed to confirm the trends indicated by the short-term tests.

THEORY

The uniform corrosion of carbon steels in geothermal brines is an electrochemical process. This means that in order for iron to corrode, some other species in the brine must be chemically reduced. The iron and the brine must be electrically coupled to permit electron flow. The anodic corrosion reaction is:

$$Fe \rightarrow Fe^{++} + 2e^{-} \qquad (1)$$

Two of the most important cathodic reactions required to complete and sustain the electrochemical corrosion process are:

$$2H^{+} + 2e^{-} \rightarrow H_2(gas) \qquad (2)$$

$$O_2 + 2H_2O + 4e^{-} \rightarrow 4OH^{-} \qquad (3)$$

Equations 2 and 3 show that the acidity (pH) and the oxygen content of the brine are very important in controlling corrosion of carbon steels. Marshall[1] and Tskhvirashvili[2] report corrosion rate control in geothermal brines is by Equation 2.

This electrochemical mechanism of carbon steel corrosion has several important implications:

- The pH of the brine at temperature is important, and corrosion will increase as acidity increases.
- Dissolved oxygen will increase corrosion.
- The presence of corrosion product films or mineral scale on the steel surfaces can slow corrosion by slowing the transport of chemical species through the scale. The composition and structure of the films on the metal surface will be important.
- Corrosion of carbon steel in dry steam will be lowered because the electrochemical cell requires water to be present.
- Temperature will be important because it changes the chemical equilibria affecting pH and changes reaction and diffusion rates.

Eh-pH Diagrams

It is very useful in both geochemistry and corrosion to plot the oxidation-reduction potential (Eh) of a system vs the pH of that system. Since Eh is related to the oxygen and redox couples in the brine, and pH to the acidity, such a diagram correlates two of the important chemical factors controlling corrosion. The Eh of a brine is related to the partial pressure of dissolved oxygen (P_{O_2}) at 25°C by:[3]

$$Eh = 1.23 + 0.0148 \text{Log } P_{O_2} - 0.059 pH \qquad (4)$$

In Figure 1[4] are plotted the Eh-pH values of many natural waters. Note that all the values are bounded by the voltage where water decomposes into oxygen at the top and hydrogen at the bottom. Natural waters near the top have much dissolved oxygen, while strongly reducing waters (such as geothermal brines) have negative values of Eh approaching the hydrogen discharge line.

It is interesting to calculate the Eh and P_{O_2} of a typical geothermal brine containing 10 ppm H_2S and 10 ppm SO_4^{-2} at pH 6 at 25°C:

$$H_2S + 4H_2O = SO_4^{-2} + 10H^+ + 8e^-$$

$$Eh = 0.303 - 0.0739 pH + 0.0074 \text{Log } \frac{(SO_4)^{-2}}{(H_2S)} \qquad (5)^*$$

$$10 \text{ ppm } H_2S = 2.94 \times 10^{-7} m$$

$$10 \text{ ppm } SO_4^{-2} = 1.04 \times 10^{-7} m$$

$$Eh = 0.303 - 0.0739\ (6) + 0.0074 \text{Log } \frac{1.04 \times 10^{-7}}{2.94 \times 10^{-7}}$$

$$= -0.143 \text{ volts}$$

*Eq. 5 from Pourbaix, 1974.

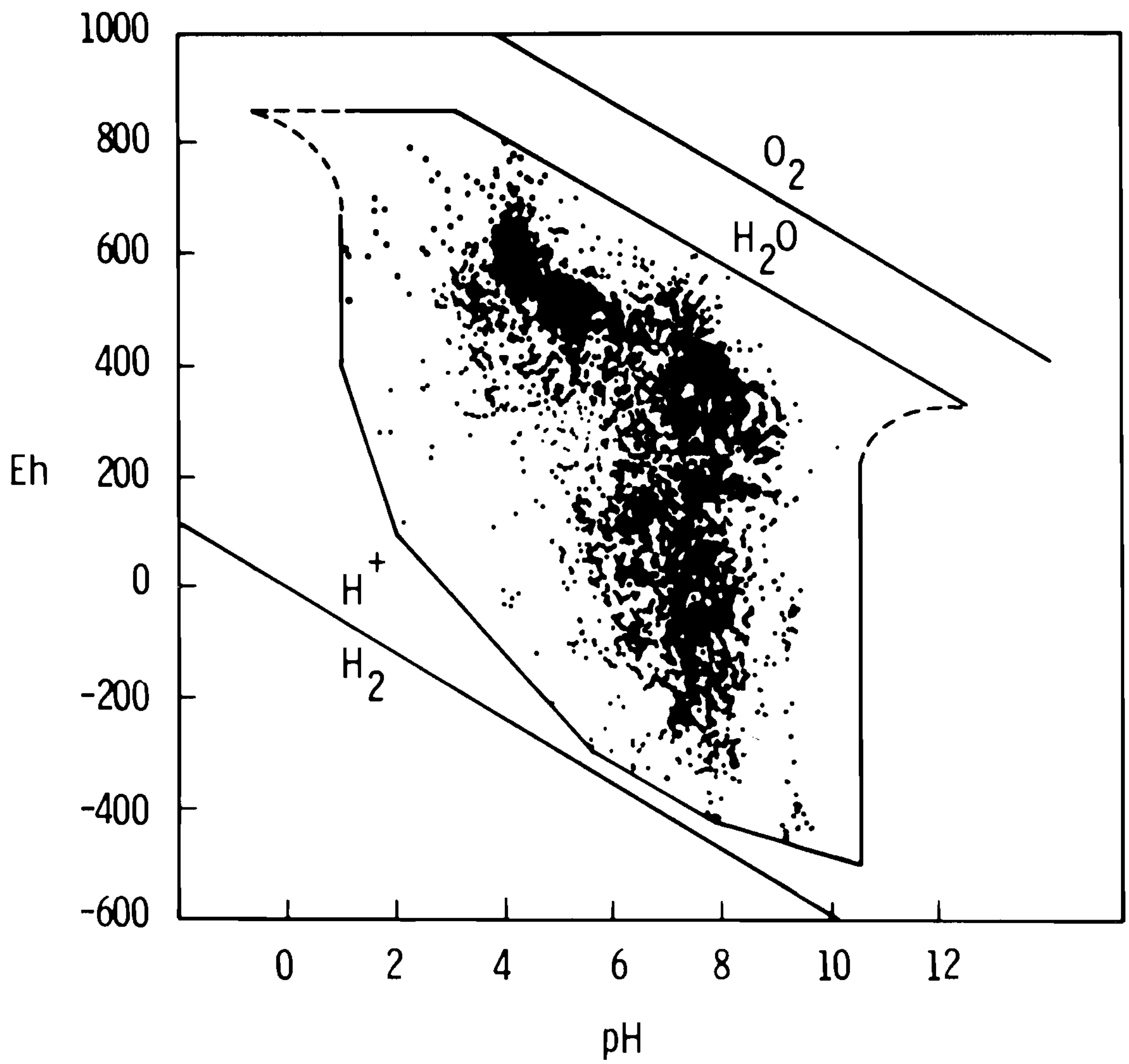

FIGURE 1. Distribution of Eh-pH Measurements of the Natural Aqueous Environments (Source: Bass, et al.)[4]

$$\text{Log}P_{O_2} = \frac{-1.23 + 0.059\text{pH} + \text{Eh}}{0.0148} \qquad (4)$$

$$P_{O_2} = 1.4 \times 10^{-69}\text{atm}$$

This oxygen value of 10^{-69}atm is so low as to only be of thermodynamic interest, but illustrates that geothermal brines containing H_2S are unlikely to contain detectable dissolved O_2 unless air inleakage occurs during or after production of fluids. If air is mixed into the brine, both H_2S and O_2 can co-exist for awhile before thermodynamic equilibrium is reestablished. However, with good plant design and operations, we could maintain the brines oxygen free and eliminate one major source of corrosion of carbon steels.

In Figure 2 (from Garrels and Christ[(6)]) a geochemical Eh-pH diagram is reproduced. It is a very useful diagram for considering corrosion of carbon steels in geothermal brines because it interrelates the thermodynamic stability of various corrosion product films on carbon steels with the Eh and pH of the brine. Most geothermal brines are buffered near neutral within ± 2 pH units, contain no dissolved oxygen and have negative Eh values. Iron oxide, iron carbonate, and iron sulfides are all possible corrosion product films depending on the specific chemistry (Fig. 2). Note that ferric ion cannot normally exist in oxygen-free geothermal brines in any measurable activity. (Fig. 2 is only valid at 25°C.)

pH at Temperature

Geothermal brines are buffered systems and the pH of the brine will depend on the specific brine chemistry together with reservoir temperature, reservoir minerals, gas content, and salinity. In Table 1 are listed some of the important acid-base equilibria that affect pH.

All of these chemical equilibria are temperature dependent. Note in Figure 3 that the carbonic acid dissociation changes by over 2 orders of magnitude from 25 to 300°C. In general, most acids become less dissociated at high temperature.

Ellis[(7)] has pointed out an important effect of salinity on pH. Because of the effects of hydrogen-alkali metal substitution in the feldspar minerals, the pH of geothermal brines tends to be buffered. As salinity increases, the increased Na^+, K^+, Ca^{+2} activities cause the H^+ activity to increase also in order to maintain chemical equilibrium with feldspar minerals (Table 1). Thus high saline geothermal reservoirs will tend to be more acidic.

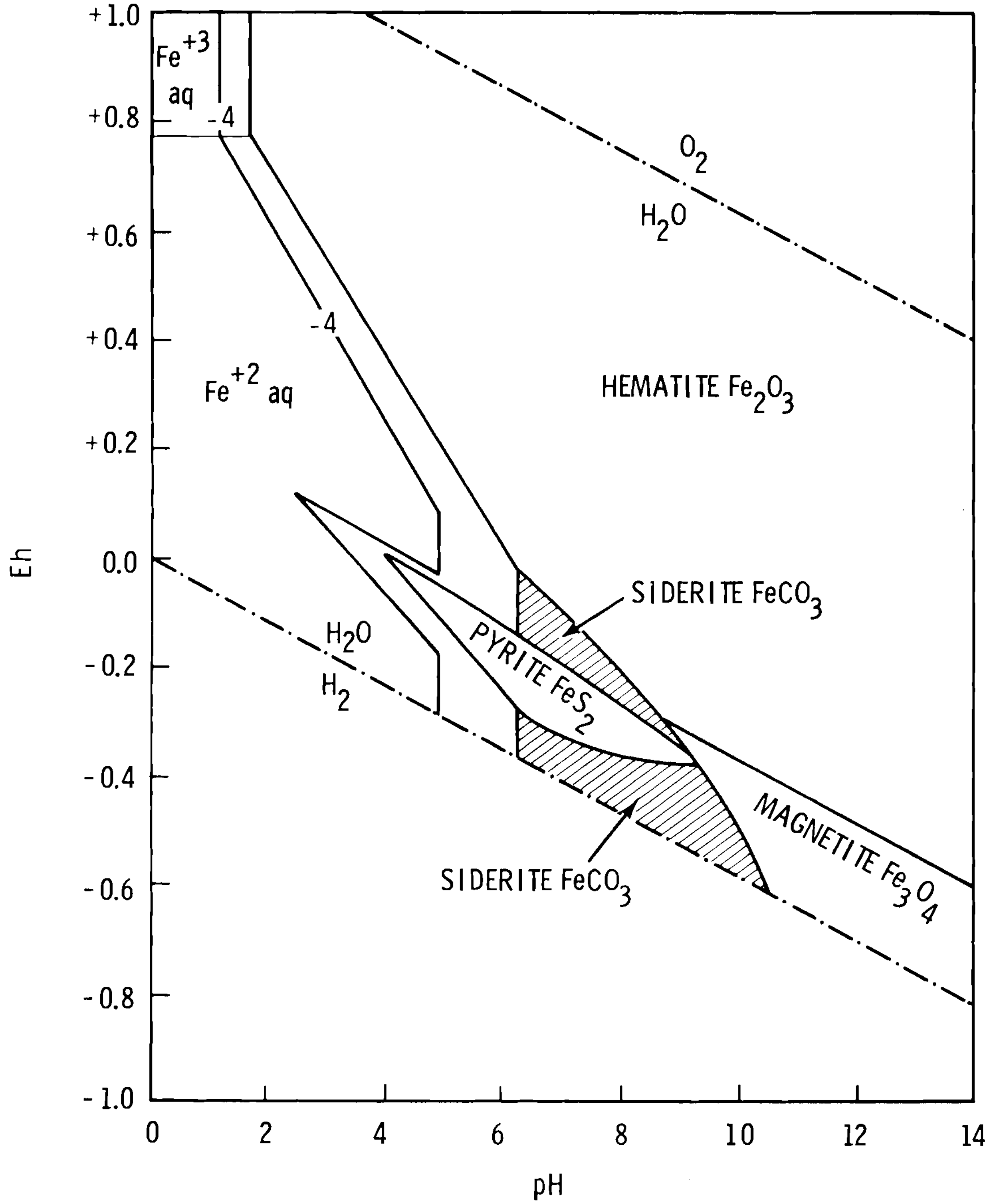

FIGURE 2. Eh-pH Diagram (25°C 1 Atm); a Sulfur = 10^{-6}; a CO_3 = 10°
(Source: Garrels and Christ)[6]

TABLE 1. Some Important Temperature Dependent Equilibria Affecting Geothermal Brine pH

$$CO_2 + H_2O \rightleftarrows H^+ + HCO_3^-$$

$$H_2S \rightleftarrows H^+ + HS^-$$

$$NH_3 + H_2O \rightleftarrows OH^- + NH_4^+$$

$$3/2\text{K-Feldspar} + H^+ \rightleftarrows 1/2\text{K-Mica} + 3SiO_2 + K^+$$

$$7\ \text{Albite} + 6H^+ + 3H_2O \rightleftarrows 3\text{Na-Montmorillinite} + 10SiO_2 + 10SiO_2 + Na^+$$

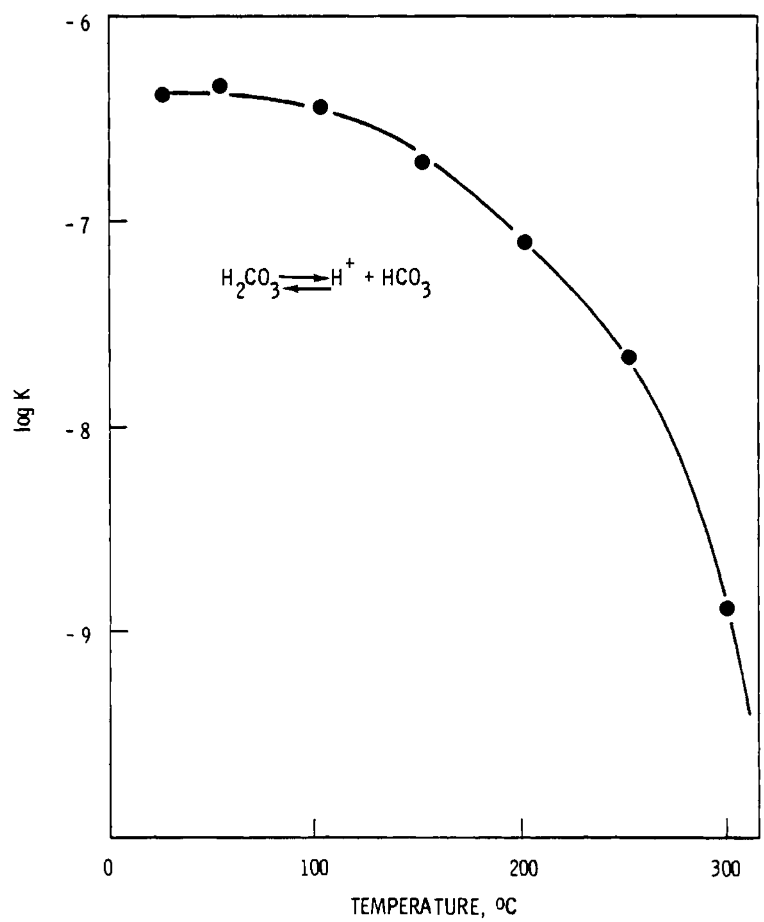

FIGURE 3. The Dissociation Constant of Carbonic Acid

When geothermal fluids are produced as two-phase water-steam mixtures, the gases CO_2, H_2S, and NH_3 fractionate almost completely to steam phase. This can cause dramatic shifts in pH in both residual brine and steam condensate. Where CO_2 controls the pH, the brine will become more alkaline and the steam condensate acidic after flashing. However, if the steam contains more NH_3 the condensate will be more alkaline. The measured pH values on field samples taken from geothermal systems can vary widely, and unless gas losses during sampling are carefully controlled, the measured pH value can be in serious error.

EXPERIMENTAL PLAN

A series of refreshed autoclave experiments were run in synthetic brines to investigate how variations in pH, temperature, salinity, silica, and H_2S levels affect the uniform corrosion of carbon steels, chromium steels, nickel alloys, titanium alloys, and zirconium (Table 2). The test series were planned to investigate the corrosion effects of varying pH at temperature at various salinities. All pH values reported were measured at 25°C; the actual pH in the test at temperature could be quite different.

These tests were to prepare background information for the interpretation of field corrosion data. We do not believe laboratory tests can ever exactly duplicate the complex chemical and surface effects controlling corrosion in real geothermal fluids. However, tests in simple brines can form a basis for interpretation of field data.

The tests were run in a refreshed Inconel 600 autoclave shown in Figure 4. Synthetic brines were made up in 300-liter batches. Oxygen was eliminated by first gas sparing with CO_2; then adding 20 to 30 ppm hydrazine. Oxygen in all brines was below analytical detection limits of 0.01 ppm oxygen.

The pH was adjusted by varying the CO_2 partial pressure in the sparge gas or by using pure CO_2 sparge gas at 1 atm pressure and adding NaOH to the tank to form bicarbonate. H_2S was added as Na_2S. Silica was added as sodium meta-silicate.

TABLE 2. Materials Studied

Carbon Steels	Carbon	Mn	P	S	Si	Ni	Cr	Mo	N	Cu	Fe	H	O	Al	Other
A570 Sheet	0.13	0.42	0.008	0.017	--	--	--	--	--	--	--	--	--	--	
A53B Pipe	0.20	0.55	0.010	0.019	0.02	0.02	0.007	0.005	--	--	Rem.	--	--	--	
SAE 1010 Tube	0.10	0.30	0.007	0.020	0.009	0.04	0.009	0.010	--	0.02	Rem.	--	--	--	
A106 Pipe	0.20	0.55	0.10	0.012	0.15	0.04	0.04	0.010	--	0.03	Rem.	--	--	--	
SAE 1010 Tube+	0.03	0.27	0.017	0.006	0.005	0.03	0.009	0.006	--	0.06	Rem.	--	--	--	
A53B Tube+	0.23	0.71	0.010	0.019	0.15	0.26	0.010	0.007	--	0.008	Rem.	--	--	--	
API Grade Well Casing Steels															
C75	0.44	1.56	0.008	0.17	0.21	--	--	0.21	--	--	Rem.	--	--	--	
C95	--	--	0.014	0.020	--	--	--	--	--	--	Rem.	--	--	--	
J55	0.41	1.08	0.011	0.013	0.08	0.03	0.03	0.004	--	--	Rem.	--	--	--	
K55	0.32	1.03	0.010	0.020	0.09	0.09	0.01	0.009	--	0.07	Rem.	--	--	--	
L80	0.29	1.22	0.021	0.033	0.07	--	--	--	--	--	Rem.	--	--	--	
N80	0.28	1.20	0.010	0.012	0.13	0.08	0.04	0.01	--	0.12	Rem.	--	--	--	
P110	--	--	0.019	0.027	--	--	--	--	--	--	Rem.	--	--	--	
Chromium Steels															
4130 Tube+	0.23	0.48	0.009	0.011	0.25	0.05	0.82	0.16	--	0.007	Rem.	--	--	--	
E-Brite 26-1	<0.001	0.020	0.010	0.011	0.21	0.14	26.23	1.0	0.010	0.020	Rem.	--	--	--	
405	0.020	0.25	0.010	0.009	0.44	0.28	13.05	0.002	--	0.051	Rem.	--	--	0.27	
410	0.12	0.20	0.009	0.014	0.27	0.24	12.23	0.05	--	0.08	Rem.	--	--	<0.01	
430	0.051	0.24	0.011	0.009	0.29	0.34	15.89	0.19	--	0.07	Rem.	--	--	0.05	
446	0.067	0.45	0.014	0.011	0.22	0.29	23.20	0.06	--	0.06	Rem.	--	--	0.02	
406	0.11	0.36	0.011	0.005	0.26	0.23	12.45	0.10	--	0.04	Rem.	--	--	1.75	
439	0.052	0.41	0.031	0.010	0.43	0.22	16.89	0.18	--	0.09	Rem.	--	--	0.11	
29-4*	0.01 max.	--	--	--	--	0.15 max.	29	4	0.02 max.	--	Rem.	--	--	--	
29-4-2*	0.01 max	--	--	--	--	2	29	4	0.02 max.	--	Rem.	--	--	--	
26-1S*	0.06 max	--	--	--	--	0.05 max	26	1	0.04 max.	--	Rem.	--	--	--	1.00 max. Ti
2-1/2 Cr, 1 Mo	0.12	0.50	0.012	0.014	0.22	0.11	2.14	1.05	--	0.18	Rem.	--	--	--	
6X*	0.03 max	1.5	--	--	--	24	20	6.5	--	--	Rem.	--	--	--	
E-Brite 26-1 Tube+	0.01	<0.10	0.015	0.011	0.18	0.09	26.2	1.06	--	0.005	Rem.	--	--	0.05	
410 Tube+	0.10	0.39	0.010	0.009	0.51	0.33	11.89	0.03	--	0.03	Rem.	--	--	0.17	
Titanium															
35-A	0.18	--	--	--	--	--	--	--	0.011	--	0.04	0.006	0.09	--	
15 Ni	0.01	--	--	--	--	1.5	--	--	0.008	--	0.04	67 ppm	0.08	--	
0.2 Pd	0.03	--	--	--	--	--	--	--	0.01	--	0.16	<100 ppm	0.122	--	0.18 Pd
6Al-4V*	--	--	--	--	--	--	--	--	--	--	--	--	--	6	4 V
Special Materials															
Hastelloy C-276*	0.02	1	0.03	0.03	0.05	Rem.	14.5-16.5	15-17	--	--	4-7	--	--	--	W 3-4.5, Co 2.5, V 0.35
Inconel 625*	0.05	0.15	--	0.008	0.25	61	21.5	9	--	--	2.5	--	--	0.2	0.2 Ti, 4 Cb
Inconel 600*	0.08	0.5	--	--	0.25	76	15.5	--	--	0.25	8	--	--	--	
Incoloy 825*	0.03	0.5	--	0.015	0.25	42	21.5	3	--	2.25	30	--	--	0.1	Ti 0.9
Zirconium*															Pure Crystal Bar

*Nominal

+Heats used in field test

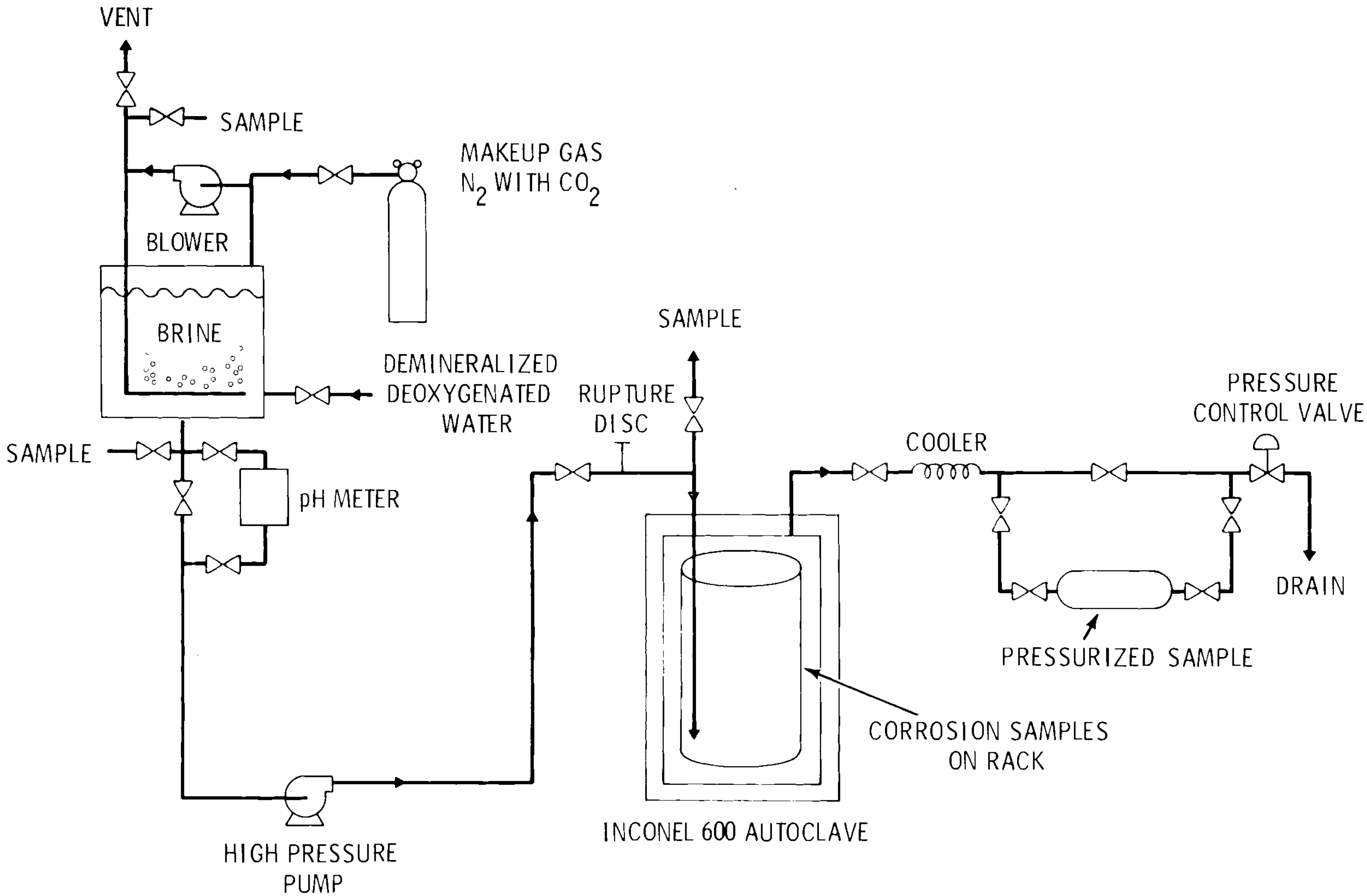

FIGURE 4. Geothermal Corrosion Test Refreshed Autoclave

Brine was pumped from these tanks at 1.5 liter/m by a high pressure pump which maintained a single phase hydraulic system in the autoclave at 68.9 Bars (1000 psig). This kept all gases in solution. The brine was dumped to drain after leaving the autoclave. This resulted in a changeout of the autoclave volume every 3.3 hours. Preliminary tests showed autoclave refreshment is essential to maintain constant chemistry, especially pH. If the autoclave is not refreshed, corrosion rates decrease.

Test coupons were used in the as-received metallurgical conditions. Surfaces of carbon steels, chromium steels and nickel alloys were prepared by mechanically grinding the surfaces, finishing with 325 grade grit paper. The titanium alloys and zirconium were etched in HNO_3-HF. All samples are weighed to 0.1 mg and areas calculated, including edges and mounting holes. Samples were exposed on Teflon insulators on a titanium rack in the autoclave for 135 hours at test conditions. One-half of the samples were removed and the remainder exposed for a second 135 hours (270 hours total). Because of the large number of alloys only one sample was used at each point. After exposure carbon steel corrosion films were stripped in inhibited 50% HCl and chromium steels and nickel alloys in an alkaline permanganate--inhibited HCl--two-step process. Only weight gain was measured for titanium alloys and zirconium.

RESULTS

The Role of pH on Corrosion

The average corrosion rates of the 10 carbon steels in 1% NaCl brines are plotted *vs* pH in Figure 5. Individual carbon steel alloy effects were minor compared to the temperature and pH effects. There is a definite pH effect observed, as expected, with corrosion increasing at lower pH values. The effect is most dramatic at 50°C however. The strong temperature dependence may be related to the higher H^+ activity at low temperature (Fig. 3), but is more likely caused by a change in corrosion film composition from no films at 50°C, to $FeCO_3$ at 150°C, to Fe_3O_4 at 250°C which was observed on X-ray diffraction patterns. These data suggest the commonly observed corrosive effects of dissolved CO_2 will become less serious at the higher temperatures observed in geothermal wells.

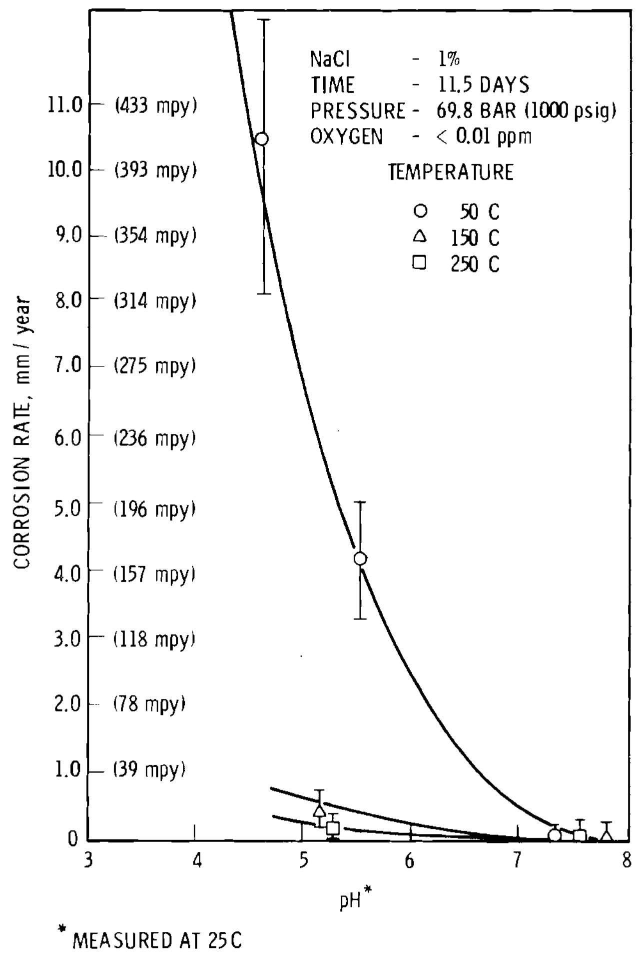

FIGURE 5. Average Corrosion of Ten Carbon Steels in NaCl-CO_2 Brines vs pH

The uniform corrosion rates of all nickel alloys, chromium steels, titanium alloys, and zirconium were 0 to 0.05 mm/yr (0 to 2 mpy) at the 1% NaCl level.

The Role of Temperature on Corrosion

The effect of temperature on corrosion in the range of 50 to 250°C was found to be interrelated with pH and salinity. In Figure 6 the average corrosion rates of 10 carbon steels are plotted vs temperature at salinities of 1% and 22% NaCl. Corrosion tended to decrease as temperature increased as more protective Fe_3O_4 was formed on the steels. However, at 250°C, as temperature and salinity both increased, corrosion rates increased.

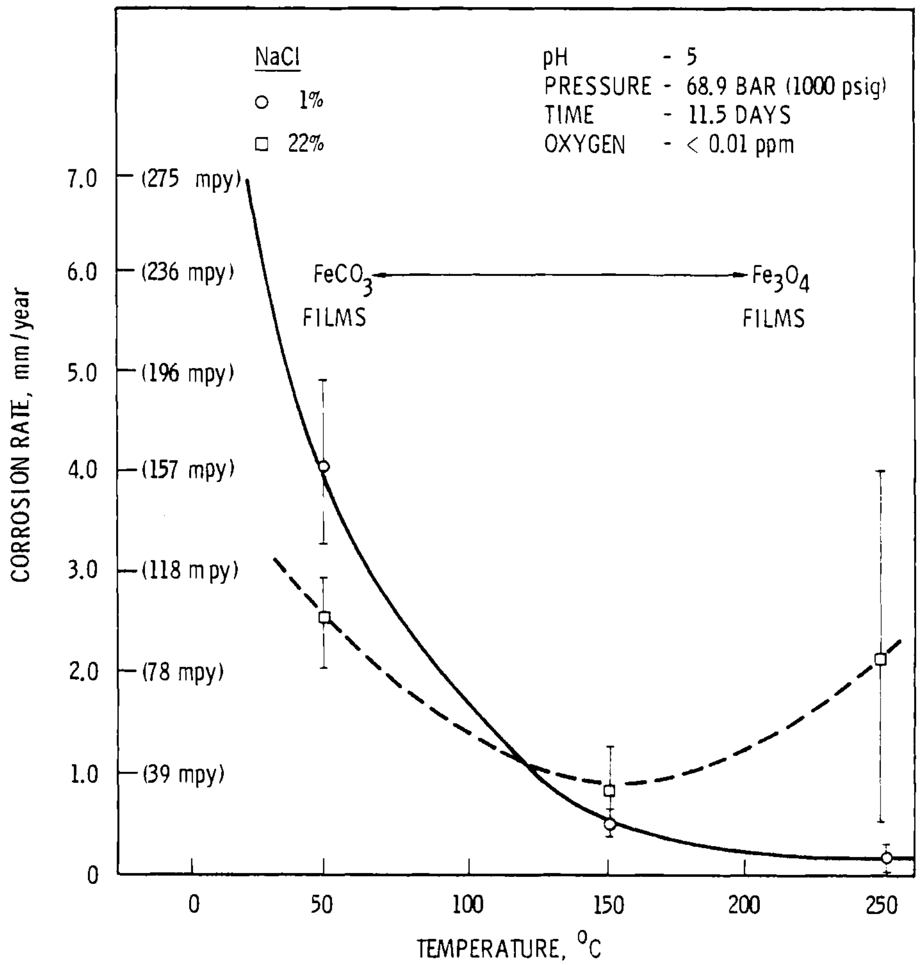

FIGURE 6. Average Corrosion of Ten Carbon Steels in CO_2-Bicarbonate Brines

The Role of Salinity on Corrosion

At temperatures of 50°C and 150°C salinity did not affect carbon steel corrosion nearly as much as pH, temperature, or film composition effects. The marked effect of salinity at 250°C was investigated separately in a test series in Figure 7. These data show a marked increase in corrosion as salinity increases up to at least 20%. The cause of this increase in corrosion appears due both to increased solution conductivity and changes in corrosion film structure. The corrosion films at 1% NaCl and 22% NaCl were both Fe_3O_4 by X-ray diffraction, however, the high salinity films were composed of fine particles rather than a coherent film. At the 10% salinity level some carbon steel alloy differences were seen in 250°C uniform corrosion as listed in Table 3.

TABLE 3. Effect of Alloy Composition on Uniform Corrosion

Temperature	250°C
Pressure	68.9 Bar (1000 psi)
Oxygen	<0.01 ppm
pH	4.6 to 4.8

	Corrosion Rate mm/yr (mpy)			
Alloy	1% NaCl	5% NaCl	10% NaCl	20% NaCl
A570	0.3 (12)	0.9 (35)	1.1 (43)	2.8 (110)
A53B Heat 1	0.3 (11)	0.6 (24)	0.9 (36)	2.8 (109)
A53B Heat 2	-	0.4 (16)	0.6 (23)	3.2 (125)
C75	0.2 (9)	0.4 (16)	0.2 (7)	2.0 (80)
1010	0.4 (14)	1.0 (38)	1.0 (41)	3.5 (136)
4130	-		0.2 (7)	2.3 (91)
2 1/4 - 1Mo	0.08(3)	0.6 (23)	0.3 (12)	1.8 (69)
410 Heat 1	0.08(3)	0.1 (4)	0.8 (30)	3.5 (137)
410 Heat 2	-	0.2 (9)	0.5 (20)	3.8 (150)
E-Brite 26-1 Heat 1	0.05(2)	0.01(0.3)	0.02(0.7)	0.08(3)
E-Brite 26-1 Heat 2	-	0.02(0.7)	0.02(0.8)	0.02(0.6)
Hastalloy C-276	0.02(0.9)	0.03(1.2)	0.04(1.7)	0.04(1.5)
Inconel 625	0.01(0.3)	0.01(0.12)	0.01(0.2)	0.02(0.8)
Inconel 600	0.02(0.6)	0.02(0.9)	0.05(1.8)	0.04(1.5)
Incoloy 825	0.01(0.4)	0.01(0.2)	0.01(0.3)	0.05(1.8)
29Cr-4-2	0.08(3)	0.01(0.2)	0.02(0.6)	0.01(0.5)
6X	0.01(0.4)	0.01(0.3)	0.01(0.3)	0.03(1.3)

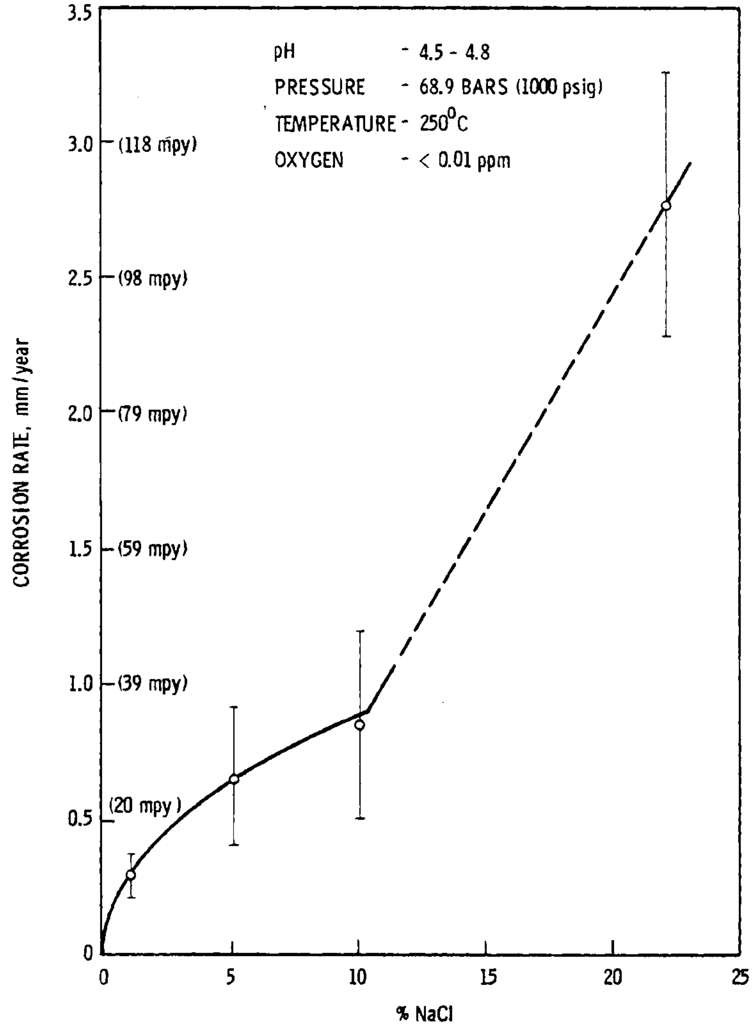

FIGURE 7. Average Corrosion Rate of Carbon Steels vs Salinity
250°C - pH 4.5-4.8
Pressure 68.9 Bars (1000 psig)
Oxygen - <0.01 ppm

The Role of Dissolved H_2S and Silica on Corrosion

The corrosion of carbon steels in 1% NaCl-CO_2 brines with either H_2S or SiO_2 additions is given in Table 4. These data indicate a slight reduction in corrosion with the addition of H_2S or SiO_2. The presence of H_2S changed the corrosion product films from $FeCO_3$ to FeS and FeS_2 at 150°C (by X-ray diffraction). While not very protective, the sulfide films were more protective than the thin carbonate films.

TABLE 4. Effect of H_2S and Dissolved Silica on Corrosion

Temperature 150°C — Pressure 68.9 Bar (1000 psig)
25°C pH 4.6 — Oxygen <0.01 ppm
NaCl 1% — Average corrosion rate mm/yr (mpy)

Alloy	1% NaCl-CO_2	1% NaCl-CO_2 + H_2S 10 mg/l	1% NaCl-CO_2 + SiO_2 400 mg/l
A570	0.53 (21 mpy)	0.53 (21 mpy)	0.41 (16 mpy)
A53B	0.53 (21)	0.41 (16)	0.36 (14)
1010	0.38 (15)	0.28 (11)	0.36 (14)
A106	0.41 (16)	0.43 (17)	0.36 (14)
C75	0.51 (20)	0.28 (12)	0.38 (15)
C95	0.58 (23)	0.33 (13)	0.38 (15)
K55	0.58 (23)	0.28 (11)	0.41 (16)
L80	0.58 (23)	0.33 (13)	0.38 (15)
P110	0.58 (23)	0.30 (12)	0.41 (16)

It was thought that the silica in solution might react with the iron to form a protective iron silicate film. The corrosion was reduced slightly with SiO_2 additions, but no silicates were identified on the surface of the one sample examined. More samples need to be studied.

The H_2S had no observable effect on any of the chromium steels, titanium alloys, or zirconium. With the nickel alloys, some sulfide corrosion took place forming nickel sulfide films on Inconel 600, with a corrosion rate of 0.25 mm/yr (10 mils/yr) at 250°C in 1% NaCl-pH 5. In the same test Hastelloy C-276 and Inconel 625 corroded only 0.01 mm/yr (0.2 mpy).

Corrosion of Alternate Alloys

The uniform corrosion of chromium, nickel, and titanium alloys and zirconium were measured along with the carbon steels. No 300 series stainless steels were included because of their well-known susceptibility to chloride stress corrosion cracking. In most of the 1% NaCl tests all the alternate alloys performed well with little uniform corrosion and no significant pitting observed. In some of the 250°C tests significant corrosion of some alloys was observed. The data in Table 5 represent the highest corrosion rates observed for the alternate alloys. The sulfide attack on Inconel 600 is the major observation with H_2S present. When exposed to high temperature, high salinity (20% NaCl) conditions, it can be seen that high chromium content above 23% is very beneficial to corrosion resistance.

Especially notable in their corrosion resistance to 250°C, oxygen free, salt brines were E-Brite 26-1, 446, the experimental high chromium alloys, nickel alloys, titanium alloys, and zirconium. Since the corrosion rates were calculated from only two samples of each alloy, minor differences in rate are not statistically significant. The aluminum containing alloy type 406 is of interest, since it showed much lower corrosion than the other 12 Cr alloys, although the corrosion was still much higher than the high chromium alloys.

Comparison of Refreshed Autoclave Data With Corrosion Rates in Actual Geothermal Brines

An obvious question is whether the trends reported for the refreshed autoclave results are applicable to real geothermal brines. To answer this question a corrosion experiment was conducted at the Bureau of Reclamation geothermal well 6-1 near Holtville, CA. This test involved a full factorial experiment of 5 alloys x 3 temperatures x 3 velocities at well head pH of 5.8 and with acid injection to lower the pH to 4.6-4.8. Only preliminary data, Tables 6 and 7, from this field test are ready at this time to provide a reference point to this paper. The data in Table 6 indicate excellent agreement on corrosion rates at 150°C in real and synthetic brines. However, the strong inverse temperature dependence on corrosion seen in the autoclave at 50°C was not confirmed in the field data. The cause of the reduced corrosion in the actual geothermal fluid at 50°C may be due to a silica film that deposited and became rate controlling. Extensive work on film composition and structure is in progress.

TABLE 5. Comparison of Alternate Alloys with Carbon Steels in Oxygen Free Brines - 68.9 Bar (1000 psig)

	250°C 1% NaCl pH 4.8 H_2S 10 mg/l	250°C - 20% NaCl pH 4.6
Average of ten carbon steels	0.18 (7 mpy)	2.2 (87 mpy)
Chromium Alloys		
2 1/4 Cr 1 Mo	0.08 (3)	0.48 (19)
E-Brite 26-1 (26 Cr-1 mo)	0.02 (0.6)	0.02 (0.6)
405 (13 Cr)	0.06 (2.5)	2.5 (98)
410 (12 Cr)	0.04 (1.4)	3.0 (120)
430 (16 Cr)	0.04 (1.7)	1.6 (62)
446 (23 Cr)	0.02 (0.7)	0.02 (0.8)
406 (12 Cr 1.8 Al)	0.06 (2.2)	0.43 (17)
439 (17 Cr)	0.04 (1.4)	0.38 (15)
29 Cr-4 Mo	0.02 (0.6)	0.02 (0.8)
29 Cr-4 Mo - 2 Ni	0.02 (0.4)	0.02 (0.8)
26 Cr-1 Mo - 1 Ti	0.02 (0.6)	0.02 (0.8)
6X - (20 Cr-24 Ni-6.5 Mo 1.5 Mn)	0.003 (0.1)	0.01 (0.5)
Nickel Alloys		
Hastelloy C-276	0.04 (1.5)	0.01 (0.5)
Inconel 625	0.005 (0.2)	0.003 (0.1)
Inconel 600	0.23 (9.2)	0.01 (0.4)
Inconel 825	0.005 (0.2)	0.008 (0.3)
Titanium Alloys		
Ti 35A	<0.005 (0.2)	<0.005 (0.1)
Ti 1.5 Ni	<0.005 (0.2)	<0.005 (0.1)
Ti 0.2 Pd	<0.005 (0.1)	<0.005 (0.1)
Ti 6 Al-4V	<0.005 (0.2)	<0.005 (0.1)
Zirconium	<0.005 (0.1)	<0.005 (0.1)

TABLE 6. Comparison of Corrosion in Refreshed Autoclave Tests with Corrosion in Actual Geothermal Brines

Corrosion Rate in mm/yr (2 week exposures)

Alloy	150°C Autoclave Test (1)	150°C Geothermal Brine (2)	50°C Autoclave Test (1)	50°C Geothermal Brine (2)
1010	0.11 (4.2 mpy)	0.15 (6.0 mpy)	0.36 (14 mpy)	0.042 (1.7 mpy)
A53B	0.12 (4.7 mpy)	0.14 (5.5 mpy)	0.46 (18 mpy)	0.045 (1.8 mpy)
4130	0.17 (6.6 mpy)	0.17 (6.8 mpy)	0.32 (12 mpy)	0.088 (3.5 mpy)
410	0.04 (1.6 mpy)	0.03 (1.3 mpy)	0.015 (0.6 mpy)	0.03 (1.3 mpy)
E-Brite 26-1	0.003 (0.1 mpy)	0.003 (0.1 mpy)	0.0067 (0.27 mpy)	0.0076 (0.3 mpy)

(1) Synthetic Brine - pH 5.6-5.8, NaCl-24,000 mg/liter, SiO_2-320 mg/liter, H_2S-1mg/liter, <0.01 ppm O_2

(2) East Mesa Well 6-1 - pH 5.6-5.8, Salinity-22,000 mg/liter, SiO_2-300 mg/liter, H_2S-1.3 mg/liter, O_2 <0.01 ppm

TABLE 7. Effect of Acidification on Corrosion in Refreshed Autoclave Tests and Actual Geothermal Brine

	Corrosion mm/yr in East Mesa 6-1 Geothermal Brine 150°C-1 ft/sec		Corrosion mm/yr in Refreshed Autoclave Tests 150°C	
Alloy	Wellhead pH 5.6 - 5.8	Acidification pH 4.6 - 4.8	pH 5.6 - 5.8	pH 4.6 - 4.8
1010	0.15 (6.0 mpy)	0.64 (25 mpy)	0.11 (4.2 mpy)	0.41 (16 mpy)
A53B	0.14 (5.4 mpy)	0.39 (15 mpy)	0.12 (4.7 mpy)	0.53 (21 mpy)
4130	0.17 (6.8 mpy)	0.56 (22 mpy)	0.17 (6.6 mpy)	--
410	0.03 (1.3 mpy)	0.04 (1.8 mpy)	0.04 (1.6 mpy)	--
E-Brite 26-1	0.003 (0.1 mpy)	0.003 (0.1 mpy)	0.003 (0.1 mpy)	--

The acid injection data (Table 7) confirmed the strong pH dependence of carbon steel corrosion where corrosion rates increased 3 to 4 times with a 1 pH unit acidification. This was the same order of change of corrosion with pH observed in the refreshed autoclave data. These acidification data are of considerable interest since acid injection is one method being considered for mineral scale control.

The 410 chromium steel and the E-Brite 26-1 showed little or no pH dependent corrosion in the field test.

The Role of Film Formation on Corrosion

We have used a thermodynamic computer code[8] to calculate what iron compound would be the stable form considering temperature, acid-base equilibria at temperature, effect of salinity on activity coefficients, and sulfur activity. These calculations are compared in Table 8 with the observed film compositions. In most cases the predicted film is near the composition that is found, indicating thermodynamic stability of the films is very important.

Refering back to Figure 2, we see the carbonate and sulfide stability fields are very important at 25°C to 50°C. Our data indicate Fe_3O_4 becomes the dominant film at 250°C. Considering the minor changes in pH, Eh, or temperature that can change the stable film composition, it is not surprising that widely varying corrosion of carbon steel is seen in geothermal systems.

We believe that the composition and structure of the corrosion film on the metal, combined with the composition and structure of the mineral scale deposits, may largely control corrosion of carbon steels in geothermal brines.

CONCLUSIONS

The large screening test of alloys in refreshed autoclave tests indicates that most common carbon steels have satisfactory uniform corrosion rates in low salinity, oxygen free geothermal brines above pH 6. Where suitable corrosion allowances are permitted, corrosion rates of carbon steels in pH 4.5 brines may be acceptable. However, the data should be used cautiously as pitting and crevice corrosion were not studied which could be important in specific cases, such as heat exchanger tubes. As temperatures and salinity

TABLE 8. Calculated Thermodynamic Stability of Iron Compounds Compared with Observed Film Composition on A570 Carbon Steel

T°C	1% NaCl, pH 7.5		1% NaCl, pH 4.8		1% NaCl, pH 4.8 + H_2S	
	Calculated	Observed	Calculated	Observed	Calculated	Observed
50	$FeCO_3$	none detected	Fe^{++}	85% Fe 10% $FeCO_3$	FeS_2	FeS
150	Fe_3O_4	Fe_3O_4	$FeCO_3$	$FeCO_3$	$FeCO_3$ FeS_2	80% $FeCO_3$ 10% FeS 5% FeS_2
250	Fe_3O_4	Fe_3O_4	Fe_3O_4	70% Fe_3O_4 + 30% $FeCO_3$	Fe_3O_4	not run

rise together, carbon steel corrosion increases to unacceptable rates at pH 5. Acidification of a slightly acid (pH 5.8) brine to pH 4.8 increased corrosion of carbon steels three to four times. The pH at temperature was found to be very important.

Films that formed on the metal generally followed thermodynamic predictions and appeared to play a major role in corrosion rate control. If this is the case, local breakdown of the film could lead to pitting attack which should be investigated further.

Except for 250°C - 20% NaCl brines, alloys with the low corrosion rates include the chromium steels containing 17 Cr or more, titanium alloys, zirconium, and nickel alloys. The titanium alloys, E-Brite 26-1, 6X and other high chromium alloys and zirconium survived every test with little more than film formation.

ACKNOWLEDGMENTS

This work was supported by the U.S. Department of Energy, Division of Geothermal Energy, R.R. Reeber, Program Manager.

The author would like to acknowledge the assistance of D.D. DeMonia and D.H. Getchell who assisted with the refreshed autoclave tests and data reductions, E.M. Woodruff who conducted the field test, and R. Wang who performed the X-ray diffraction analyses. S.J. Thompson assisted with the field test data.

We would like to acknowledge U.S. Steel Corporation, Allegheny Ludlum Steel Corporation, International Nickel Company, Stellite Division, Cabot Corporation, and Airco Vacuum Metals who provided samples of commercial production materials for this study.

REFERENCES

1. T. Marshall and A. J. Hugill, "Corrosion by Low Pressure Geothermal Steam." Corrosion, Vol. 13, p. 329, May 1957.

2. D. Tskhvirashvili, et al., "On Corrosion of Metals in Geothermal Power Plants." Geothermics, Vol. 1, No. 3, p. 113, 1972.

3. Garrels and Christ, Solutions Minerals, and Equilibria. Harper and Row, p. 177, 1965.

4. Bass, Becking, et al., Journal Geology, 68, p. 243, 1960.

5. M. Pourbaix, "The Atlas of Electrochemical Equilibria in Aqueous Solutions." NACE, Houston, TX, 1974.

6. Garrels and Christ, Solutions Minerals, and Equilibria. Harper and Row, p. 224, 1965.

7. A. J. Ellis, "Quantitative Interpretation of Chemical Characteristics of Hydrothermal Systems." Geothermics, Special Issue 2, p. 516, 1970. Proceedings of the U.N. Symposium on the Development and Utilization of Geothermal Resources, Pisa, 1970.

8. D. W. Shannon, J. R. Morrey and R. P. Smith, "Use of a Chemical Equilibrium Code to Analyze Scale Formation and Corrosion in Geothermal Brines." Proceedings of International Symposium on Oilfield and Geothermal Chemistry, SPE 6592, p. 21, June 27-29, 1977.

DISTRIBUTION

No. of Copies	
	UNITED STATES
	A. A. Churm DOE Chicago Patent Group Argonne, IL 60439
16	R. R. Reeber Division of Geothermal Energy Department of Energy Washington, D.C. 20545
1	John V. Walker Division of Geothermal Energy Department of Energy Washington, D.C. 20545
	George A. Kolstadt U.S. Department of Energy Division of Basic Energy Sciences Washington, D.C. 20545
531	DOE Technical Information Center
	Harold Bell Arizona Public Service Co. P.O. Box 21666 Phoenix, AR 85036
	Jay F. Kunze Aerojet Nuclear Company 550 Second Street Idaho Falls, ID 83401
	Richard L. Miller Aerojet Nuclear Company 550 Second Street Idaho Falls, ID 83401
	Jack R. Maurer Allegheny Ludlum Steel Corp. Research Center Brackenridge, PA 15014

No. of Copies	
	J. Baldwin Allied Chemical Corporation 550 Second Street Idaho Falls, ID 83401
	John Bond Barber Nichols Engineering Co. 6325 W. 55th Avenue Arvada, CO 80002
	Jerome W. Hankin Bechtel Corporation 50 Beale Street San Francisco, CA 94105
	Edward L. Ghormley The Ben Holt Co. 301 S. Lake Avenue Pasadena, CA 91101
	Ben Holt The Ben Holt Co. 201 S. Lake Avenue Pasadena, CA 91101
	Jose Samaniego The Ben Holt Co. 201 S. Lake Avenue Pasadena, CA 91101
	Thomas M. Laronge Betz Environmental Engineers, Inc. 9317-J Highway 99 Vancouver, WA 98665
	Larry Kukacka Brookhaven National Laboratory Upton, NY 11973
	Wayne A. Fernelius Bureau of Reclamation Region 3 Boulder City, NV 89005

No. of
Copies

George A. Frye
Burmah Oil & Gas Co.
P.O. Box 11279
Santa Rosa, CA 94506

A. R. Troiano
Case Western Reserve University
Cleveland, OH 44106

F. W. Schremp
Chevron Oil Field Research Co.
P.O. Box 446
La Habra, CA 90631

John E. Howard
Department of Water and Power
City of Los Angeles
Water and Power Square
Room 1136A
111 N. Hope St.
Los Angeles, CA 90051

Coury and Associates
7400 W. 14 ave. Suite 2
Lakewood, CO 80214

Hector Alonso
Commission Federal de Electridad
Planta Cerro Prieto
P.O. Box 248
Calexico, CA 92281

Samuel Poredes
Commission Federal de Electridad
Planta Cerro Prieto
P.O. Box 248
Calexico, CA 92281

Alfredo Manon
Commission Federal de Electridad
Planta Cerro Prieto
P.O. Box 248
Calexico, CA 92281

John S. Wilson
Dow Chemical Company
Texas Division
Freeport, TX 77541

No. of
Copies

Dr. Hunter Pallman
Dow Chemical Company
2800 Mitchell Dr.
Walnut Creek, CA 94598

A. C. Makrides
EIC Corporation
55 Chapel St.
Newton, MA 02158

P. N. LaMori
Electric Power Research Institute
P.O. Box 10412
Palo Alto, CA 94304

V. Roberts
Electric Power Research Institute
P.O. Box 10412
Palo Alto, CA 94304

G. Underhill
Electric Power Research Institute
P.O. Box 10412
Palo Alto, CA 94304

Dawn Jacobs
Exxon Production Research
P.O. Box 2189
Houston, TX 77001

Stanley G. Unitt
Fluor Engineers and
Constructor, Inc.
3333 Michelson Drive
Irvine, CA 92715

Geothermal Resources Council
P.O. Box 1033
Davis, CA 95616

Merrill Cohen
General Electric Company
Medium Steam Turbine Dept.
1100 Western Avenue
Lynn, MA 01910

No. of
Copies

H. Tsui Meidav
Geonomics, Inc.
3165-7 Adeline Street
Berkeley, CA 94703

Thomas C. Hinrichs
Imperial Magma
P.O. Box 2082
Escondido, CA 92025

B. R. Banerjee
Ingersol Rand Company
Research Center
P.O. Box 301
Princeton, NY 08540

Richard A. McKay
Jet Propulsion Laboratory
4800 Oak Grove Drive
Pasadena, CA 91103

C. M. Laffoon
C. M. Laffoon Consulting
P.O. Box 1892
El Cajon, CA 92022

John A. Apps
Lawrence Berkeley Laboratory
University of California
Berkeley, CA 94720

Kenneth F. Mirk
Lawrence Berkeley Laboratory
University of California
Berkeley, CA 94720

Sidney L. Phillips
Lawrence Berkeley Laboratory
University of California
Berkeley, CA 94720

3 George Tardiff
Lawrence Livermore Laboratory
P.O. Box 808
Livermore, CA 94551

No. of
Copies

Arthur L. Austin
Lawrence Livermore Laboratory
P.O. Box 808
Livermore, CA 94551

Morton C. Smith
Los Alamos Scientific Laboratory
P.O. Box 1663
Los Alamos, NM 87544

Harry W. Falk, Jr.
Magma Power Company
P.O. Box 9
Los Altos, CA 94022

Reinald Nielsen
The Mitre Corporation
Bedford, MA 01730

Martin School
The Mitre Corporation
Energy Resource & Environmental System Analysis
Westgate Research Park
McLean, VA 22101

E. R. Fuller
National Bureau of Standards
Materials Building
Washington, D.C. 20234

R. B. Coryell
National Science Foundation
Geothermal Energy Studies
1800 G Street
Washington, D.C. 20550

John W. Arlidge
Nevada Power Company
P.O. Box 230
Las Vegas, NV 89151

R. Lyon
Oak Ridge National Laboratory
P.O. Box X
Oak Ridge, TN 37830

No. of
Copies

R. W. Bowman
Oilwell Research, Inc.
2419 E. Main Street, Suite E
Ventura, CA 93003

Geo-Heat Utilization Center
Oregon Institute of Technology
Klamath Falls, OR 97601

Paul Mathew
Pacific Gas & Electric Co.
77 Beale
San Francisco, CA 94105

John Finney
Pacific Gas & Electric Co.
77 Beale
San Francisco, CA 94105

Gordon W. Allen
Pacific Gas & Electric Co.
3400 Crow Canyon Road
San Ramon, CA 94583

Frank J. Dodd
Pacific Gas & Electric Co.
3400 Crow Canyon Road
San Ramon, CA 94583

H. K. McCluer
Pacific Gas & Electric Co.
3400 Crow Canyon Road
San Ramon, CA 94583

Hubert L. Barnes
Pennsylvania State University
208 Deike
University Park, PA 16802

Gary W. Crosby
Phillips Petroleum Company
11526 Sorrento Valley Road
San Diego, CA 92121

Alan D. Grant
Portland General Electric
121 S.W. Salmon Street
Portland, OR 97204

No. of
Copies

Art Martinez
Public Service Co. New Mexico
P.O. Box 2267
Albuquerque, NM 87103

David. W. DeBerry
Radian Corporation
P.O. Box 9948
Austin, TX 78766

James E. Murphy
Reno Metallurgy Research Center
U.S. Bureau of Mines
1605 Evans Avenue
Reno, NV 89505

Dr. James Barkman
Republic Geothermal, Inc.
11823 E. Slauson Avenue, Suite 1
Santa Fe Springs, CA 90670

Michael J. Walker
Republic Geothermal, Inc.
11823 E. Slauson Avenue, Suite 1
Santa Fe Springs, CA 90670

James Kuwada
Rogers Engineering
16 Beale Street
San Francisco, CA 94105

Leslie F. Wohlberg
Rogers Engineering
16 Beale Street
San Francisco, CA 94105

Gyan P. Hajela
Rockwell International
Atomics International Division
8900 DeSoto Avenue
Canoga Park, CA 91304

Thomas Springer
Rockwell International
Atomics International Division
8900 DeSoto Avenue
Canoga Park, CA 91304

No. of Copies

Howell E. White
The Rust Engineering Company
P.O. Box 101
Birmingham, AL 35201

Digby McDonald
Stanford Research Institute
Menlo Park, CA 94025

Barry Syrett
Stanford Research Institute
Menlo Park, CA 94025

Sandia Corporation
Albuquerque, NM 87115

H. K. Bishop
San Diego Gas & Electric Co.
P.O. Box 1831
San Diego, CA 92112

Gilbert L. Lombard
San Diego Gas & Electric Co.
P.O. Box 1831
San Diego, CA 92112

William O. Jacobson
San Diego Gas & Electric Co.
P.O. Box 1831
San Diego, CA 92112

Peter R. Rhodes
Shell Development Company
P.O. Box 1380
Houston, TX 77001

Lynn Rasban
Southern California Edison
P.O. Box 800
Rosemead, CA 91770

Donald J. Truax
Standard Oil Company of California
Materials Laboratory
Richmond, CA 94802

No. of Copies

Paul Kruger
Stanford University
Civil Engineering Dept.
Stanford, CA 94305

Frank W. Dickson
Stanford University
Department of Geology
Stanford, CA 94305

David Anderson
California Resources Conservation Development Commission
State of California
Sacramento, CA 95814

Edward Gravelle
Sundstrand Fluid Handling
2480 West 70th Avenue
Denver, CO 80221

L. L. Sluzalis
Sundstrand Fluid Handling
2480 West 70th Avenue
Denver, CO 80221

Richard S. Treseder
6272 Girvin Drive
Oakland, CA 94611

Joseph M. Kennedy
TRW
One Space Park
Redondo Beach, CA 90278

Robert Wheatley
Union Oil Research Center
P.O. Box 76
Brea, CA 92621

L. J. P. Muffler
U.S. Department of Interior
Office of Geochemistry and Geophysics
345 Middlefield Road
Menlo Park, CA 94025

No. of
Copies

Paul B. Needham
U.S. Department of the Interior
U.S. Bureau of Mines
College Park, MD 20740

R. O. Fournier
U.S. Department of Interior
Office of Geochemistry and
Geophysics
345 Middlefield Road
Menlo Park, CA 94025

J. D. Gibson
U.S. Department of Interior
Alaska Resources Library
555 Cordova Street
Anchorage, AK 99501

W. Ogle
U.S. Department of Interior
3801 B. West 44th Avenue
Anchorage, AK 99503

Charles A. Reedy
United Chemical Company
145 W. 16th Street
Long Beach, CA 90813

Val Finlayson
Utah Power and Light Company
P.O. Box 899
Salt Lake City, UT 84110

Kenneth R. Starling
University of Oklahoma
School of Chemical Engineering
and Materials Science
Norman, OK 73069

Bruce Heath
University of Oklahoma
School of Petroleum
Engineering
Norman, OK 73069

No. of
Copies

Myron H. Dorfman
University of Texas
Center for Energy Studies
Austin, TX 78712

University of Hawaii at Monoa
2424 Maili Way
Honolulu, HI 96822

Otto Vetter
3189 C Airway Avenue
Costa Mesa, CA 92626

W. C. Wolkenhauer
Washington Public Power
Supply System
3000 Geo. Washington Way
Richland, WA 99352

FOREIGN

Jorge Guiza
Commission Federal
de Electridad
Dept. of Geothermal Resources
Mexico 5, D.F. Mexico

Sergio Mercado
Commission Federal
de Electridad
Dept. of Geothermal Resources
Mexico 5, D.F. Mexico

CNUCE
Istintuto Del Consiglio
Nazionale Delle Ricerche
36 Via S. Maria/56100
Pisa, Italy

Russell James
Department of Scientific and
Industrial Research
Taupo, New Zealand

Japan Geothermal Energy
Association
Yurakucho Denki Building
1-7-1 Yuraku-Cho Chiyoda-Ku
Tokyo, Japan

No. of
Copies

ONSITE

DOE Richland Operations Office

H. E. Ransom

Battelle-Northwest

C. H. Bloomster
R. A. Clark
M. J. Danielson
L. J. Defferding
R. L. Dillon
W. S. Kelly
R. P. Marshall
W. R. McSpadden
L. T. Pederson
L. H. Parry
D. W. Shannon (30)
R. P. Smith
R. G. Sullivan
J. W. Upton
R. A. Walter
J. C. Watson
E. M. Woodruff (5)
Technical Information (5)
Technical Publications